

Diverse Cellular Functions of the Hsp90 Molecular Chaperone Uncovered Using Systems Approaches

Amie J. McClellan,^{1,4} Yu Xia,^{3,5} Adam M. Deutschbauer,² Ron W. Davis,² Mark Gerstein,³ and Judith Frydman^{1,*}

¹Department of Biological Sciences

²Department of Biochemistry

Stanford University, Stanford, CA 94305, USA

³Department of Molecular Biophysics and Biochemistry, Yale University, New Haven, CT 06520, USA

⁴Present address: Division of Natural Sciences, Bennington College, Bennington, VT 05201, USA.

⁵Present address: Bioinformatics Program, Department of Chemistry, Boston University, Boston, MA 02215, USA.

*Correspondence: jfrydman@stanford.edu

DOI 10.1016/j.cell.2007.07.036

SUMMARY

A comprehensive understanding of the cellular functions of the Hsp90 molecular chaperone has remained elusive. Although Hsp90 is essential, highly abundant under normal conditions, and further induced by environmental stress, only a limited number of Hsp90 “clients” have been identified. To define Hsp90 function, a panel of genome-wide chemical-genetic screens in *Saccharomyces cerevisiae* were combined with bioinformatic analyses. This approach identified several unanticipated functions of Hsp90 under normal conditions and in response to stress. Under normal growth conditions, Hsp90 plays a major role in various aspects of the secretory pathway and cellular transport; during environmental stress, Hsp90 is required for the cell cycle, meiosis, and cytokinesis. Importantly, biochemical and cell biological analyses validated several of these Hsp90-dependent functions, highlighting the potential of our integrated global approach to uncover chaperone functions in the cell.

INTRODUCTION

Protein folding and assembly in the cell often requires the assistance of a diverse set of enzymes known as molecular chaperones. The major chaperone systems in the eukaryotic cytosol, Hsp70, TRiC/CCT, and Hsp90, are each essential for viability, suggesting that they fulfill non-overlapping functions (Frydman, 2001; Young et al., 2004). Despite intensive mechanistic and functional studies, the spectrum of cellular substrates and functions mediated by these different chaperones remains largely undefined. A better characterization of the division of labor among

different chaperone systems is key to understanding the underlying logic of cellular protein folding. The recent identification of Hsp90 as a promising target for anticancer therapies also highlights the practical implications of understanding the extent of chaperone function in the cell (Whitesell and Lindquist, 2005).

Hsp90 is the central component of a complex chaperone system whose cellular functions and mechanism are still poorly understood (Pearl and Prodromou, 2006; Young et al., 2004). In higher eukaryotes, Hsp90 collaborates with a large set of cochaperones to mediate the conformational regulation of tyrosine kinases and steroid hormone receptors (reviewed in Buchner, 1999; Picard, 2006; Young et al., 2001). Hsp90 has also been proposed to buffer phenotypic variation of these signaling molecules, allowing cells to maintain a wild-type phenotype in the face of genetic mutations (Sangster et al., 2004). The structures of Hsp90 and several Hsp90 cofactors have recently been elucidated (Pearl and Prodromou, 2006), but it is still unclear how this chaperone recognizes its substrates or affects their conformation.

Biochemical and genetic approaches suggest that Hsp90 is not a general chaperone for newly synthesized proteins. An important open question is whether the cellular function of Hsp90 is restricted to the conformational regulation of the limited set of substrates or “clients” identified to date. Considering that Hsp90 constitutes ~1%–2% of cytosolic proteins and is essential for viability in yeast, which lack tyrosine kinases and steroid hormone receptors, it is likely that Hsp90 performs as yet unidentified cellular functions. Additionally, the precise contribution of Hsp90 in protecting cells from stress remains undefined (Nathan et al., 1997). Thus, while Hsp90 levels are highly induced by environmental stress, it is required neither to confer thermotolerance nor to prevent the aggregation of heat-inactivated proteins (Nathan et al., 1997). Traditional biochemical and genetic approaches to define chaperone substrates in vivo have been hindered by many factors, including the low affinity of most

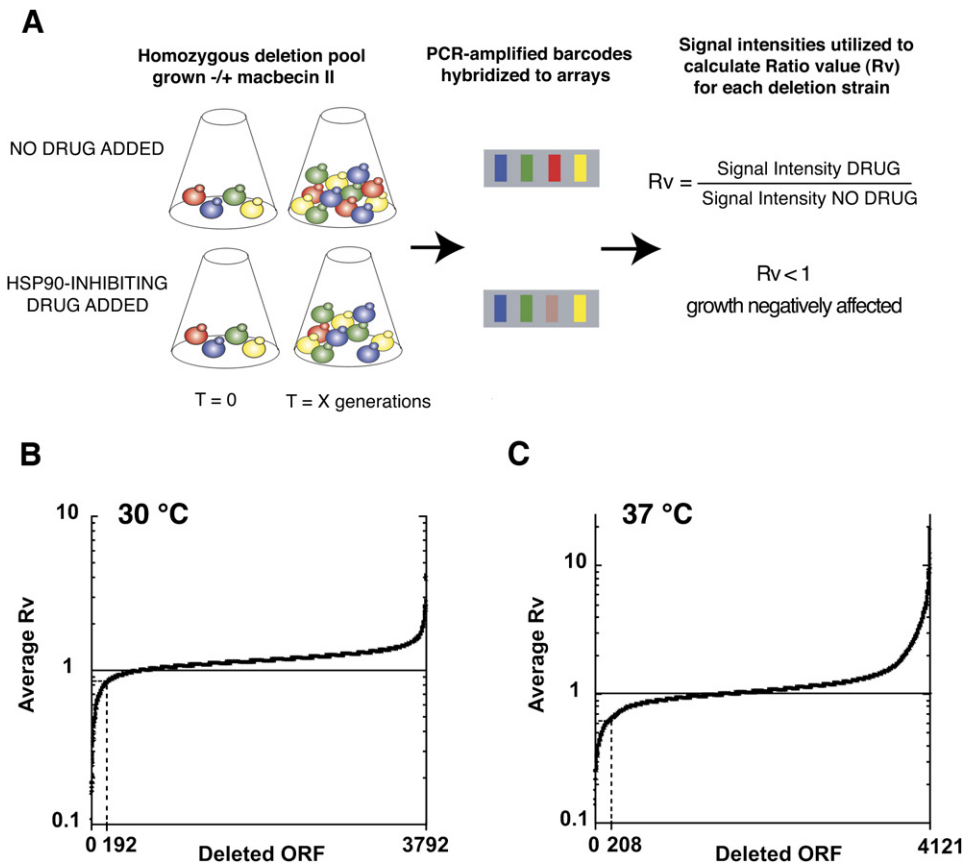


Figure 1. Experimental Scheme and Graphical Representation of Homozygous Deletion Pool Data

(A) Pooled homozygous diploid deletion strains comprising most nonessential ORFs were grown in the absence (no drug added) or presence (HSP90-inhibiting drug added) of Macbecin II. A deletion strain hypersensitive to the loss of Hsp90 function (depicted in red) will grow less robustly than unaffected strains upon drug addition. Upon subsequent hybridization of PCR-amplified molecular barcodes to complementary high-density oligonucleotide arrays, decreased signal intensity correlates with decreased presence of that particular strain in the pool. The resulting Ratio values (R_v) describe how the growth of each deletion strain was affected by HSP90 inhibition.

(B) Each deletion strain (deleted ORF) was plotted versus the averaged R_v from five independent 30°C experiments. The top 5% most growth-inhibited strains were selected as the data set for further study (average $R_v \leq 0.86$; 192 ORFs).

(C) Each deletion strain (deleted ORF) was plotted versus the averaged ratio values (R_v) from three independent 37°C experiments. Again, the top 5% constitutes the data set for further study (average $R_v \leq 0.65$; 208 ORFs).

chaperone-substrate interactions and the pleiotropic and essential nature of chaperone action. The emergence of global methods of analysis may provide an avenue to overcome some of these problems. However, these methods also present significant shortcomings, most notably the limited confidence level of many of the measurements and the difficulties of extracting coherent and significant conclusions from such large amounts of data. A few genomic studies have explored the function of Hsp90 using TAP pull-downs, two-hybrid interaction, synthetic genetic arrays (SGA), and chemical-genetic screening of a haploid yeast deletion collection (Millson et al., 2005; Zhao et al., 2005). These screens yielded several potential Hsp90 interactors: two new “client” proteins, the kinases Hog1p and Sit2p, and two new cochaperones, Tah1p and Pih1p, both containing the known Hsp90-interacting TPR domain. While each of these different global approaches

identified potential Hsp90 interactors, they did not produce an integrated picture of the cellular functions of Hsp90. The limited overlap between potential targets produced by the different approaches further underscores the limitations of genome-wide screens.

To define the cellular functions of Hsp90, we combined genomic screens that produce quantitative high-confidence data with in-depth bioinformatic analyses (Figure 1). This strategy produced novel and unexpected insights into Hsp90-dependent cellular processes both under normal growth conditions and during environmental stress. We find that, under normal growth conditions, Hsp90 facilitates protein secretion and trafficking. In addition, during environmental stress, Hsp90 is required for progression of the cell cycle, meiosis, and cytokinesis. Importantly, biochemical and cell biological approaches validate some of the Hsp90-dependent functions revealed in our screen.

Given the potential of Hsp90 as an anticancer target, a better understanding of Hsp90 functions may facilitate the design of better therapeutic strategies. Further, the efficacy of this combined approach in uncovering Hsp90 function may lay the groundwork for a comprehensive analysis of chaperone function *in vivo*.

RESULTS

Experimental Approach: Genome-wide Screen for Hsp90 Function

A chemical-genetic screen using diploid yeast collections containing precise deletions of each open reading frame (ORF) (Winzeler et al., 1999) and a pharmacological inhibitor of Hsp90 (Bohen, 1998) was used to generate a quantitative measure of deletion strains whose growth is negatively affected when Hsp90 function is compromised at either 30°C or 37°C (Figure 1). Each deletion strain is marked by kanamycin resistance and flanked with a unique “molecular barcode.” A pool containing all homozygous deletion strains was grown in the presence of an Hsp90-inhibiting drug and quantitatively analyzed by hybridization of the identifier barcodes to a high-density oligonucleotide array (Giaever, 2003). Screening the homozygous diploid deletion pool offers significant advantages over similar approaches using the haploid deletion collection strains. For example, haploid strains in the deletion collection are known to harbor secondary mutations unlinked to the kanamycin integration cassette (Deutschbauer et al., 2005). The use of the diploid collection genetically masks such recessive background mutations. Given its proposed role in buffering genetic variation, this consideration is particularly relevant for Hsp90, as growth defects in haploid cells upon Hsp90 inactivation may also arise from secondary mutations. Importantly, the yeast cytosolic Hsp90 proteins are the only targets of the Hsp90 inhibitors used in this study, as *S. cerevisiae* lacks the endoplasmic reticulum (ER) Hsp90-homolog Grp94.

We initially determined the effective concentration(s) of Hsp90-inhibiting drug macbecin II (herein MII) using a yeast strain deleted for *STI1/HOP* (Hsp Organizing Protein), a known cochaperone of Hsp90. We employed MII instead of the related and more widely used geldanamycin because MII is more effective *in vivo* in yeast cells while retaining specificity for Hsp90 (Bohen, 1998). We reasoned that deletion of the known Hsp90 cochaperone *STI1*, combined with inhibition of Hsp90 function, would result in decreased fitness of *sti1*Δ cells grown in solution. Indeed, while the growth of WT yeast was similarly affected by either 200 μM or 400 μM MII, *sti1*Δ yeast exhibited a dose-dependent decrease in growth rate (Figure S1A in the Supplemental Data available with this article online). These experiments therefore established an MII concentration range that selectively uncovers gene deletions that are hypersensitive to Hsp90 impairment, without producing unwanted cytotoxic effects on strains that are less dependent on Hsp90 function.

We next grew pooled homozygous diploid deletion strains, representing the majority of all nonessential ORFs, in the absence and presence of MII (Figure 1A). To gain insight into Hsp90 function under normal and stress conditions, experiments were carried out at both 30°C (i.e., normal) and 37°C (i.e., thermal stress) growth temperatures. The pooled strains were grown for five generations, then diluted into fresh media and grown for an additional five generations (Figure S1B). Genomic DNA prepared from cells collected after ten generations of growth was hybridized on arrays containing unique molecular barcodes identifying each deletion strain. Importantly, the relative strength of the signals obtained with and without drug for each deletion strain was used to derive a Ratio value, or Rv, which provides a quantitative measure of the effect of Hsp90 impairment on the growth rate of each strain (see Figure 1A and Experimental Procedures). This Rv served as a marker of the impact of the experimental condition on the fitness of each deletion strain (Giaever et al., 2002). Thus, an Rv < 1 indicates a growth defect when Hsp90 is inhibited (Figure 1A and Experimental Procedures). As a critical control, we confirmed for several individual deletion strains identified in our screen that the deletion rendered them susceptible to chemical inhibition of Hsp90 outside of the context of being grown in a pool (Figures S1 and S2).

The global impact of inhibiting Hsp90 was next assessed by plotting the Rv value (Figure 1A) of each deleted ORF in the pool (Figures 1B and 1C) to generate a picture of the overall fitness of strains in the pool (Table S1). Most deletion strains had an Rv equal to or greater than 1, indicating that they were not hypersensitive to Hsp90 inhibition (Figures 1B and 1C). Of the small fraction of strains negatively affected by Hsp90 inhibition (Rv < 1), we selected the top 5% most sensitive deletion strains for further analysis. The resulting 30°C data set consists of 192 genes, all with an Rv ≤ 0.86. Analysis of the 37°C data set yielded 208 genes, all with an Rv ≤ 0.65. Notably, while 90 genes were present in both data sets, there were significant differences between the Hsp90-dependent strains identified at either temperature (Figure 2A).

Bioinformatic Analyses of Hsp90 Target Data Sets Enrichment of Known Hsp90 Interactors

Yeast contains two Hsp90 proteins, one encoded by the stress-inducible *HSP82* locus and one by the constitutively expressed *HSC82* locus. While both the 30°C and 37°C data sets contain the *hsp82*Δ/*hsp82*Δ deletion strain, *hsc82*Δ/*hsc82*Δ yeast did not exhibit decreased fitness in the presence of MII. It thus appears that, even though Hsc82 and Hsp82 are nearly identical proteins (95% identity, 99% conservation) and are expressed at comparable levels in either the presence or absence of MII (data not shown), they are not functionally equivalent *in vivo*.

Next, we compiled a list of known Hsp90 interactors (Hsp90 interactome; Table S2) from data available in the BioGRID database (see Experimental Procedures).

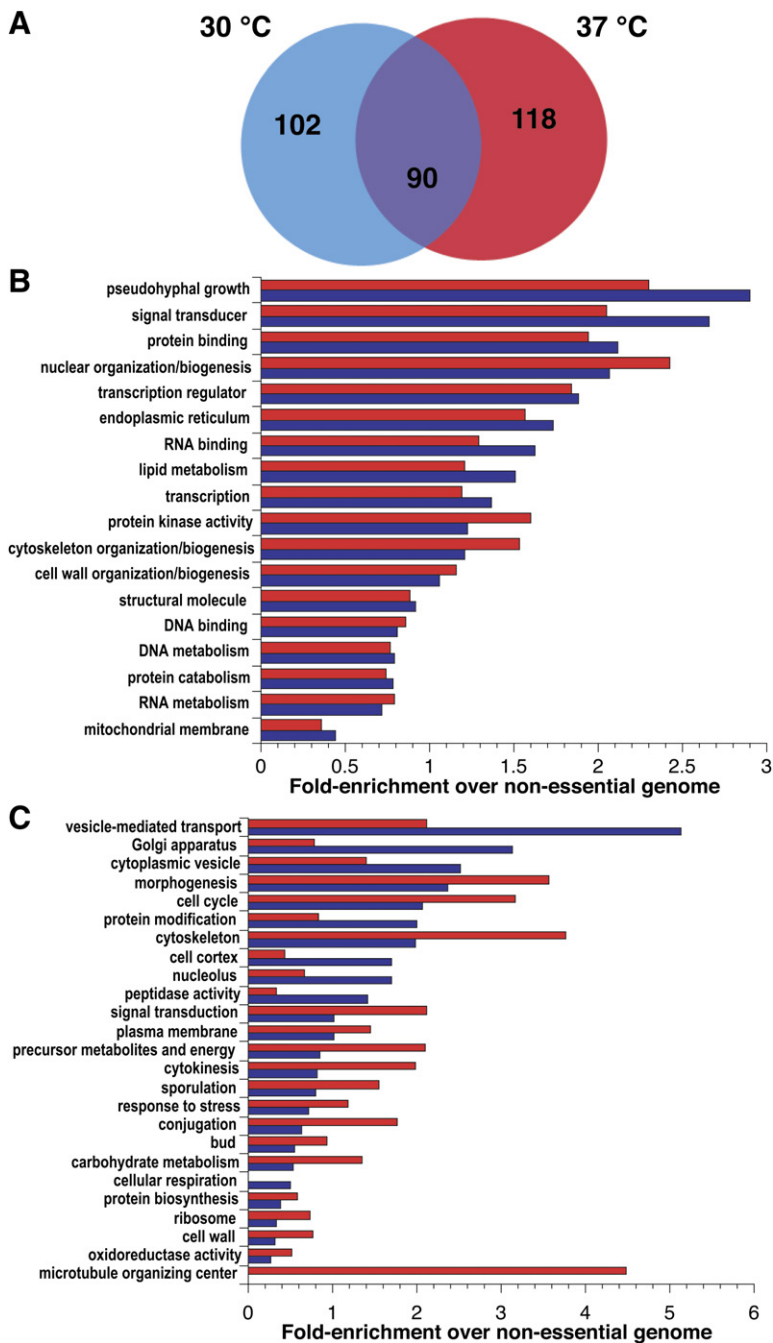


Figure 2. Overall Properties of the 30°C and 37°C Hsp90 Targets in the Homozygous Deletion Collection

(A) Degree of overlap between the data sets from 30°C and 37°C experiments.

(B) GO Slim compartment, function, and process categories were similarly significantly enriched in both the 30°C (blue bars) and 37°C (red bars) top 5% data sets. Selection criteria were (1) a value ≥ 0.7 and ≤ 1.3 upon dividing 30°C enrichment by 37°C enrichment and (2) more than one ORF assigned to at least one of the two top 5% data sets.

(C) GO Slim compartment, function, and process categories that exhibit a distinct enrichment change comparing the 30°C (blue bars) and 37°C (red bars) top 5% data sets selected as in (B), but for values < 0.7 or > 1.3 .

Both the 30°C and 37°C data sets were significantly enriched in Hsp90 interactome members (Table 1). For instance, several high-confidence nonessential Hsp90 interactors, such as HSP82 itself and the cochaperones ST11, CPR6, and SBA1, were 1.9 times more likely to be found in our screens than other Hsp90 targets, and 4.5 times more likely to be found in our screens than a random protein. Importantly, given that our study essentially represents a synthetic genetic analysis using a small-molecule inhibitor to perturb Hsp90 function, the observed enrichment for genetically established interactors

indicates that our data sets likely comprise bona fide cellular targets of Hsp90.

Identification of Cellular Activities Enriched among Hsp90 Targets

We next determined whether our data sets were enriched in genes involved in specific cellular activities using available classifications from the Gene Ontology (GO) database (Harris et al., 2004). To this end, the proportion of genes in the MII-sensitive data sets assigned to a specific GO classification was compared with the proportion of all nonessential genes with the same assignment (Tables S3

Table 1. Hsp90 Data Sets Are Significantly Enriched for Known Hsp90 Interactors

Growth Temperature	ORFs Analyzed	Known Hsp90 Targets Analyzed		Known Hsp90 Targets in Top 5%		Enrichment Ratio ^a		Significance (p Value)	
		Genetic	All	Genetic	All	Genetic	All	Genetic	All
30°C	3792	178	415	39	55	4.3	2.6	1 × 10 ⁻¹²	4 × 10 ⁻¹²
37°C	4121	204	458	41	56	4.0	2.4	1 × 10 ⁻¹²	6 × 10 ⁻¹¹

^aEnrichment ratio calculated as ((known Hsp90 interactors in top 5%)/[all top 5% ORFs])/([known Hsp90 interactors analyzed]/[all analyzed ORFs]).

and S4). This analysis revealed that some cellular functions were indeed significantly enriched among Hsp90 targets. For the most significantly enriched GO classifications, at least 80% of the genes assigned to each particular GO classification were identified in our 30°C experimental data set (Table S3, for 30°C $p \leq 0.0002$, fold enrichment ≥ 15.8). GO Slim analysis for compartments, functions, and processes enriched in both the 30°C and 37°C data sets revealed categories including transcription factors, kinases, and mitochondrial membrane components (Figure 2B). These target classes are in good agreement with previously established Hsp90-dependent “clients” and functions (Picard, 2002; Pratt and Toft, 2003; Wegele et al., 2004). The correspondence between GO analysis and known Hsp90 functions indicates that GO categories may be useful to uncover novel cellular functions of Hsp90.

We next analyzed GO Slim categorizations differentially enriched at either 30°C or 37°C degrees. The Hsp90 30°C data set was significantly enriched in transport-related categories, including vesicle-mediated transport and Golgi apparatus (Figure 2C, blue bars; see also Table S5). For instance, the 25 most sensitive strains in the 30°C screen included 14 transport-related genes, including multiple *VPS* genes and all four lobe B components of the bilobular conserved oligomeric Golgi (COG) complex (Ungar et al., 2002; Table S1). The striking enrichment of components of the secretory pathway in our 30°C data set is also evident in Table S4 ($p \leq 0.002$; fold enrichment ≥ 3), suggesting that, under normal growth conditions, Hsp90 plays an important role in protein trafficking.

To obtain insight into the function of Hsp90 during stress, we next focused on GO Slim analysis of the 37°C data set, which, strikingly, identified a different set of Hsp90-dependent processes (Figure 2C and Table S5). For instance, while components of the microtubule organizing center were not enriched in the 30°C data set, they were dramatically enriched at 37°C (4.5-fold enrichment over genome frequency; Figure 2C, red bars). Similarly, signal transduction, cell cycle, cytokinesis, and bud components, while enriched in the 30°C data set, were more abundantly represented at 37°C. The 37°C data set was also more enriched over the 30°C data set in some metabolism-related categories as well as, understandably, response to stress (Figure 2C, red bars). Thus, at elevated temperatures Hsp90 appears to play

an important role in the continued function of the cell cycle machinery as well as in the maintenance of certain types of enzymatic activities.

Role of Hsp90 in Complex Assembly

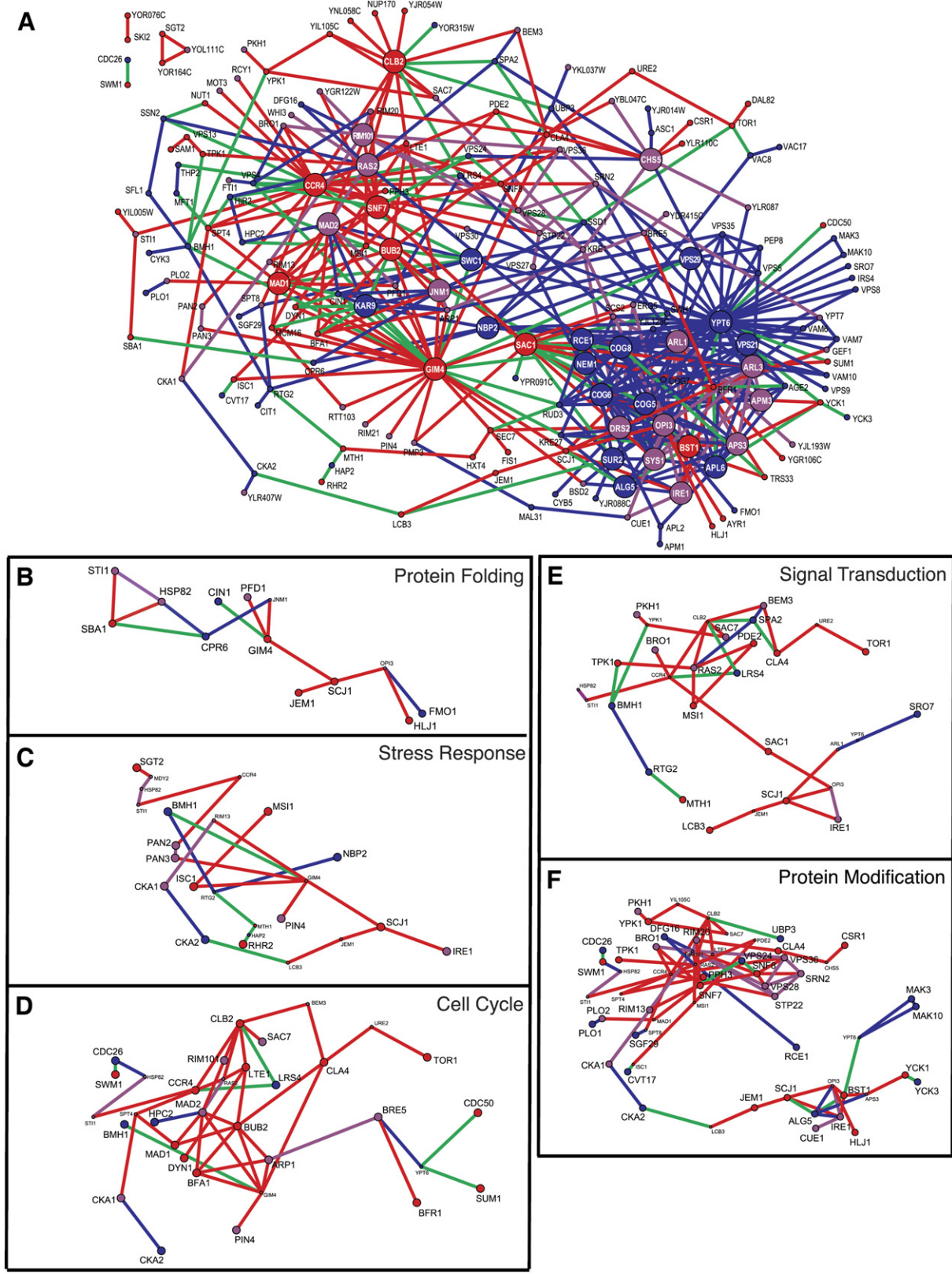
Molecular chaperones can also facilitate assembly of oligomeric complexes (Frydman, 2001; Young et al., 2004). To determine whether Hsp90 plays a role in complex formation, we assessed the enrichment of complex-forming proteins in the 30°C and 37°C data sets (see Experimental Procedures). Notably, there was a significant enrichment in genes encoding subunits of oligomeric complexes among ORFs unique to the 30°C data set; 50% of Hsp90 targets encoded subunits of oligomeric complexes, compared to 30.4% of all ORFs analyzed at 30°C. For instance, Hsp90 targets include genes coding for subunits of the oligomeric complexes COG, AP-adaptor, and ESCRT, all of which function in the secretory pathway (see also Table S7 and Figure 6B). Notably, this enrichment was not observed in the 37°C data set; only 36.4% of ORFs unique to the 37°C data set are found in complexes, compared to 32.4% of all ORFs analyzed at 37°C. Thus, Hsp90 may function to stabilize or facilitate formation of oligomeric complexes at 30°C; this function appears to be less relevant during thermal stress.

Enrichment of Structural Domains among Hsp90 Interactors

Bioinformatic analysis using Pfam classifications to determine whether certain structural domains are enriched in our experimental data sets yielded less defined trends. However, several Pfam classes were enriched over background (p value ≤ 0.034 ; Table S6). These included several designations, including TPR domain-containing proteins and DnaJ-type proteins that are known to interact with Hsp90; thus, other categories enriched in our data sets, such as the small GTPase domain found in Ras, Rabs, and Arfs (see below) may also be relevant as either substrate- or cochaperone-interacting motifs.

Network Analysis of Hsp90 Interactions

We next constructed an Hsp90 interaction network by combining our data sets with curated physical and genetic interactions from the BioGRID database (Stark et al., 2006) (Figure 3A; see Experimental Procedures). Hsp90 targets present in the 30°C, 37°C, or both data sets were grouped according to their shortest distance to Hsp90. Loner nodes (107 ORFs out of the 310 total unique



ORFs in our data sets) are not considered here, but these as yet “unconnected” Hsp90 targets may represent an unmined area of potential novel Hsp90 interactors. Graph-theoretic analysis of Hsp90 targets in relation to the yeast interaction network revealed that the average shortest distance between Hsp90 targets is smaller than expected from random chance (see [Experimental Procedures](#); [Figure S3A](#)). Accordingly, the number of gene pairs that directly interact or were next-to-nearest neighbors were much larger than expected for both the 30°C and 37°C data sets. For instance, the 30°C data set contained 306 gene pairs with one step distance between them, i.e., connected by one edge, while the expected number was 23.9 (p value < 0.001); in addition, we observed 4629 gene pairs that are two steps/edges in distance but expected only 869.5 (p value < 0.001 ; [Figure S3A](#)). The observation that the genes identified in our screen are clustered in the yeast interaction network indicates that Hsp90 targets tend to interact with each other.

The nonrandom nature of our experimental Hsp90 interaction network was further underscored when the yeast interaction network was integrated with our experimental Hsp90 data sets to determine the network distance (i.e., 0, 1, 2, etc., interactions away) between Hsp90 itself and each Hsp90 target. The average distance to Hsp90 of Hsp90 targets in both the 30°C and 37°C data sets was smaller than expected by chance (see [Experimental Procedures](#); [Figure S3B](#)). This analysis further strengthens the conclusion that our experimental data sets identified cellular targets of Hsp90.

The overall interactive character of our Hsp90 network was further evaluated by statistically analyzing the occurrence of major nodes of interaction, or hubs, defined as proteins with more than 25 interaction partners. Using this criterion, approximately 20% of all yeast ORFs function as hubs. Hsp90 targets contained higher than expected numbers of hubs. We observed a 3.2 enrichment ratio (p value $\leq 10^{-12}$) for hubs in the 30°C data set. At 37°C this enrichment was less pronounced, albeit significant (enrichment ratio 2.5; p value $\leq 10^{-12}$). These results emphasize the highly interactive nature of Hsp90 targets. The enrichment of hubs at 30°C may correlate with our observation that the 30°C data set is enriched in components of multiprotein complexes. The connectivity of Hsp90 targets was further exploited by extracting from the global Hsp90 network subnetworks of genes assigned to specific GO categories (protein folding, stress response, cell cycle, signal transduction, and protein modification; [Figures 3B–3F](#)). Interestingly, the protein modification sub-

network ([Figure 3F](#)) contains not only expected Hsp90-dependent targets such as kinases (i.e., YCK1, YCK3, CKA1, CKA2), but also the ER-associated IRE1 and CUE1, members of the ERAD/UPR pathways, suggesting a link between Hsp90 and ER quality control. This subnetwork also includes ubiquitin-dependent protein trafficking components, as well as nearly all subunits of the multivesicular body sorting pathway ESCRT I, II, and III complexes. Of note, another ESCRT III complex member, DID4, ranked numerically at 213 in the 37°C data, just outside the cutoff for the 206 ORFs comprising the data set for analysis.

In summary, our network analysis reveals that Hsp90 does not interact with a random set of genes and its function is not required for random cellular processes. Rather, Hsp90 targets tend to lie in similar protein complexes, functional clusters, or pathways, yielding a modular interaction network. Interaction subnetworks extracted from this graphic analysis further underscore the role of Hsp90 in specific cellular activities, including cell cycle regulation and cellular transport pathways.

Experimental Validation of Cell Cycle Progression and Secretion as Two Major Housekeeping Functions of Hsp90

Combining the graph-theoretical analysis of our data sets with GO analysis uncovered the modular nature of the Hsp90 interaction network ([Figure 4A](#)). This graphic analysis highlights two major functional modules in the network, suggesting a role for Hsp90 in cellular trafficking and transport, as well as in cell cycle regulation. We next sought to experimentally validate these putative roles of Hsp90.

First, we focused on the link between Hsp90 and cell division. Yeast harboring a mutant allele of Hsp90 (G313S) as their sole source of Hsp90 function exhibited morphological abnormalities consistent with defective cell cycle progression ([Figure 4Bi](#), compare WT *HSP82* to *hsp82* G313S). The cell cycle defect of Hsp90-impaired cells was also apparent when WT and G313S yeast were synchronized and analyzed by flow cytometry. While yeast containing WT Hsp90 have clear G1 and G2 populations, G313S yeast have no defined G1 peak and appear to be largely arrested as 2N cells ([Figure 4Bii](#), FACS). Consistent with these results, fluorescence microscopy indicated that, in contrast to WT cells, G313S cells had an aberrant morphology, often with both nuclei in only one of the two cells, or with unequally distributed DNA ([Figure 4Bii](#), *hsp82* G313S inset, arrow and asterisk, respectively).

Figure 3. Hsp90 Interaction Network and Associated Cellular Processes

(A) Interaction network generated from curated protein-protein and genetic interactions (see [Experimental Procedures](#)) within the 30°C and 37°C data sets. Blue nodes represent deletion strains in the 30°C data set, red nodes represent genes in the 37°C data set, and purple nodes indicate genes in both the 30°C and 37°C data sets. Blue edges connect blue nodes to blue or purple nodes, red edges connect red nodes to red or purple nodes, purple edges connect purple nodes, and green edges connect red nodes to blue nodes. Highly interactive experimental nodes or hubs (defined as ≥ 25 interactions within the network) are enlarged and labeled in white. (B–F) Subnetworks of prevalent GO processes contained within the Hsp90 interaction network: protein folding (B), stress response (C), cell cycle (D), signal transduction (E), and protein modification (F). Nodes assigned to each GO process are enlarged and labeled with enlarged font. Shown are all possible shortest-distance paths within the subnetwork between assigned nodes, as well how each subnetwork links back to Hsp90 (*HSP82*).

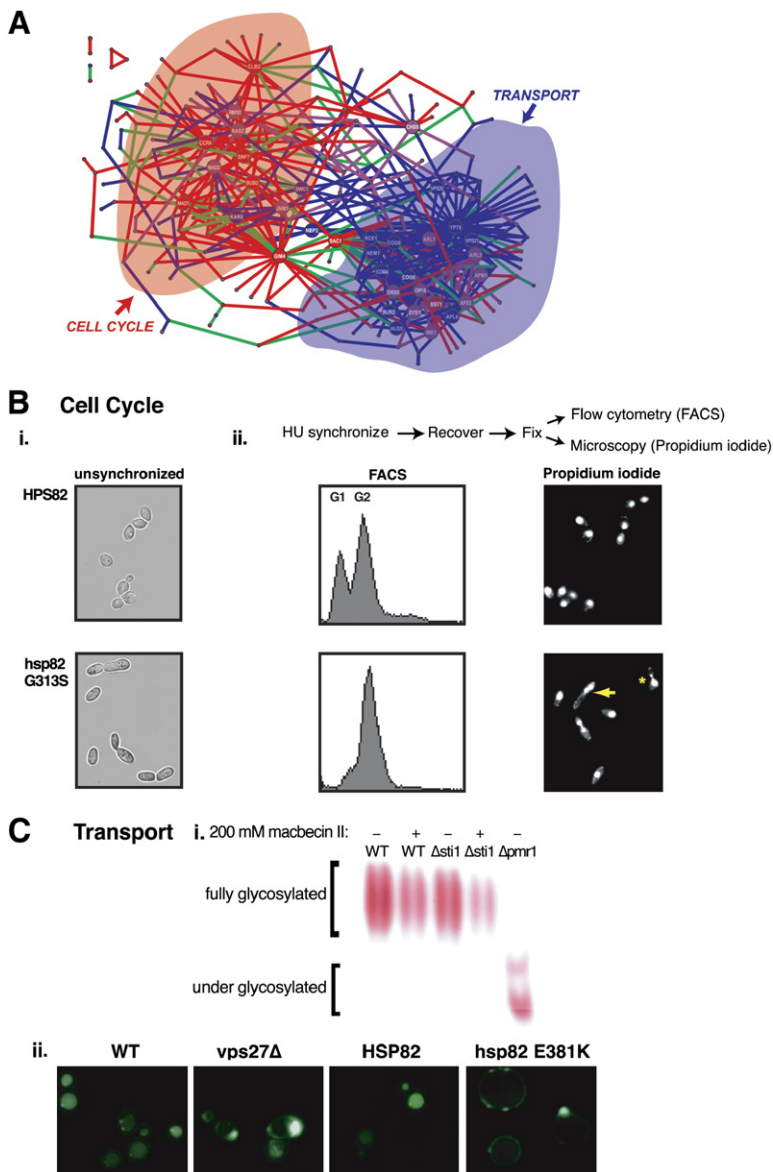


Figure 4. Biological Validation of Roles for Hsp90 in the Cell Cycle and in Cellular Transport

(A) The two main functional modules of the Hsp90 interaction network, cell cycle and protein transport, are highlighted.

(B) (Bi) Unsynchronized WT (*HSP82*) and mutant (*hsp82* G313S) yeast were morphologically examined with bright-field microscopy (100×). (Bii) WT (*HSP82*) and mutant (*hsp82* G313S) yeast were synchronized with hydroxyurea and subsequently fixed and stained with propidium iodide for analysis by flow cytometry (FACS) and microscopy (propidium iodide; 100×). Arrow indicates dividing yeast with both nuclei remaining in mother cell. Asterisk highlights an example of unequal DNA division.

(C) (Ci) WT or *sti1Δ* yeast were grown under low-glucose conditions in the absence or presence of MII and analyzed for secreted invertase activity with an in-gel assay. *pmr1Δ* yeast were included as a control for defective invertase glycosylation. The migratory positions of fully glycosylated and underglycosylated invertase are indicated. (Cii) Yeast deleted for *VPS27* (Δ *vps27*) or the isogenic wild-type strain (WT), as well as yeast with a mutant Hsp90 allele (*hsp82* E381K) or the parental allele (*HSP82*) were transformed with a GFP-Carboxypeptidase-S (GFP-CPS) expression plasmid and analyzed by fluorescence microscopy.

Our bioinformatic analysis also suggested a role for Hsp90 in vesicular transport. To test this prediction, we employed a general assay for protein secretion. Growing yeast in low glucose induces a secreted form of the enzyme invertase that acquires oligosaccharide modifications as it transits through the ER and Golgi apparatus (Figure 4Ci). MII treatment of either WT or *sti1Δ* cells dramatically reduced the amount of active invertase secreted to the media (Figure 4Ci). Of note, Hsp90 impairment did not have an observable effect on the glycosylation state of either the secreted (Figure 4Ci) or the intracellular (data not shown) invertase, unlike the loss of glycosylation observed in *pmr1Δ* cells lacking a Golgi-localized manganese pump (Luk and Culotta, 2001). This finding supports the notion that Hsp90 is required for proper secretory pathway function.

Network and GO analysis of our data sets also linked Hsp90 to several complexes involved in protein vacuolar targeting, including *VPS27*, which encodes a cysteine-rich protein (Piper et al., 1995), and *BSD2*, an ER membrane protein involved in metal homeostasis (Liu and Culotta, 1994). Several components of the ESCRT I, II and III complexes, which participate in the multivesicular body pathway (Katzmann et al., 2003), were also present in our data sets (Table S7; Figure 6B). These bioinformatic analyses prompted us to test experimentally if indeed Hsp90 function is required for proper trafficking to the vacuole. To this end, we examined the subcellular localization of GFP fused to Carboxypeptidase S (CPS) (Katzmann et al., 2003). When sorting of CPS into the lumen of the vacuole is compromised, as in *vps27Δ* deletion strains, CPS mislocalizes to the outer, limiting

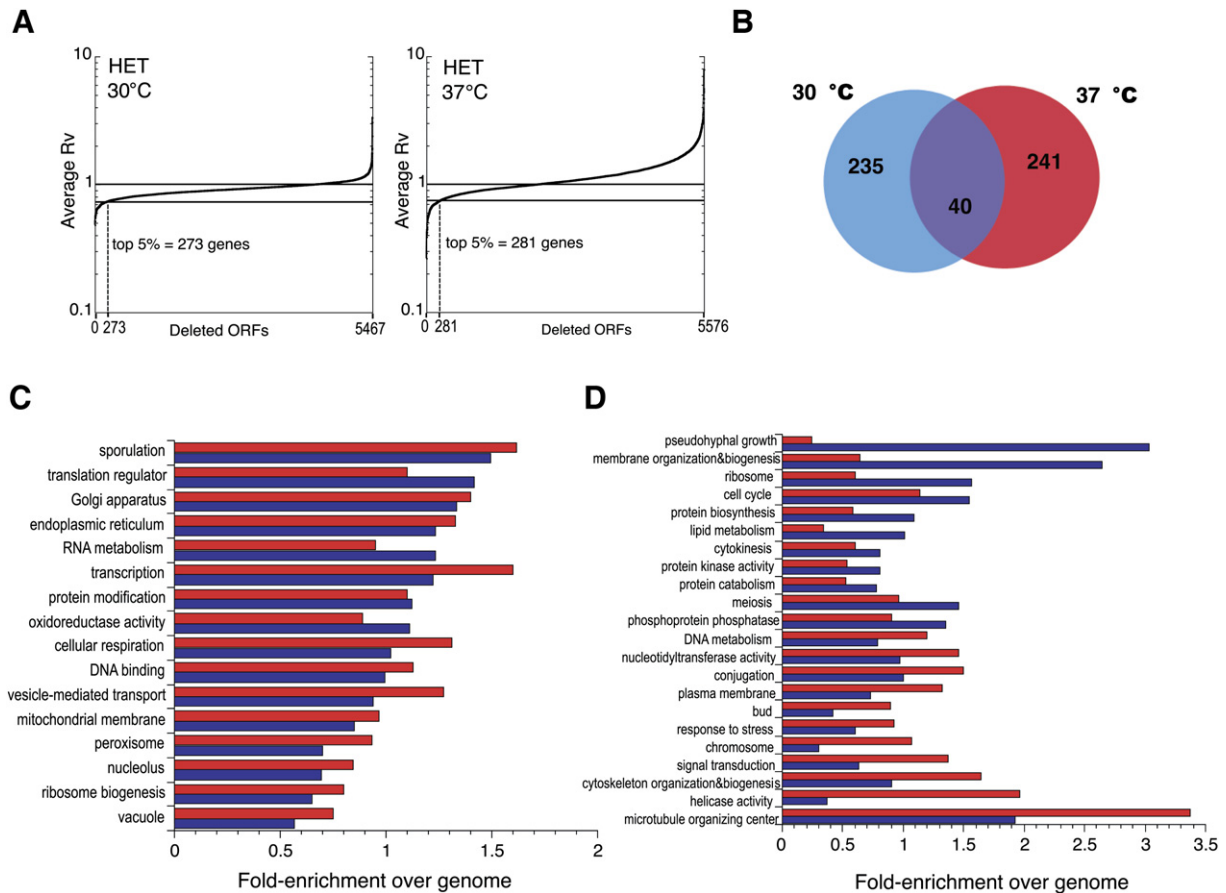


Figure 5. Overall Properties of the 30°C and 37°C Hsp90 Targets in the Heterozygous Deletion Collection

(A) Each deletion strain (deleted ORF) was plotted versus the averaged ratio values (Rv) from three independent 30°C and 37°C experiments. The top 5% of strains exhibiting a growth defect at 30°C (average Rv \leq 0.74395; 273 ORFs) or 37°C (average Rv \leq 0.74946; 281 ORFs) were selected as the data sets for further study.

(B) Degree of overlap between the top 5% data sets from heterozygous deletion pool 30°C and 37°C experiments.

(C) Comparison of GO Slim compartment, function, and process categories that are similarly significantly enriched in both the 30°C (blue bars) and 37°C (red bars) data sets. All assignments shown have (1) a value \geq 0.7 and \leq 1.3 upon dividing 30°C enrichment by 37°C enrichment and (2) more than one ORF assigned to at least one of the two data sets.

(D) Comparison of GO Slim compartment, function, and process categories that exhibit a distinct enrichment change comparing the 30°C (blue bars) and 37°C (red bars) data sets. Selection criteria mirror those described in (C), but for values $<$ 0.7 or $>$ 1.3.

membrane of the vacuole and accumulates in aberrant endosome-like structures (Hettema et al., 2004; Katzmann et al., 2003; Odorizzi et al., 2003) (Figure 4Cii). While GFP-CPS localized correctly to the lumen of the vacuole in cells containing a WT Hsp90 allele, cells harboring the E381K mutant allele of Hsp90 (Nathan et al., 1997) exhibited a sorting defect similar to that of yeast lacking *VPS27* (Figure 4Cii). Thus, Hsp90 function is indeed required for proper trafficking of proteins into the vacuole.

The agreement between these experiments and the conclusions of our bioinformatic analysis of the whole-genome screens validates the basic premise of this study, namely that the integration of genomic, computational, and network analyses may constitute a powerful tool to uncover the underlying logic of the chaperone machinery.

In particular, we uncover that Hsp90 is required for both cell cycle progression and cytokinesis and for proper function of the secretory pathway.

Comprehensive Network Analysis of Hsp90 in the Secretory Pathway

The global analysis of Hsp90 function using the homozygous diploid deletion collection necessarily overlooks essential genes. To better define Hsp90 involvement in protein secretion, we extended our analysis by performing a similar screen on the heterozygous diploid deletion collection, which contains barcode-tagged deletions in one allele of both essential and nonessential genes.

The experimental strategy for the screen and analysis of the resulting data sets was essentially as described for the homozygous deletion screen (Figure 5A, 30°C, 37°C;

Table S8). The resulting 30°C heterozygous top 5% data set consists of 273 ORFs, all with an average $R_v \leq 0.744$, and the 37°C data set contains 281 ORFs with an average $R_v \leq 0.749$. As observed for the homozygous screen, the 30°C and 37°C data sets exhibited only partial overlap (40 ORFs; Figure 5B).

Analysis of the data sets using available GO Slim classifications (Table S9; Figure 5CD) revealed that, as observed for the homozygous deletion screen, some cellular functions were significantly enriched among Hsp90 targets at both temperatures (Figure 5C), while there were also noteworthy differences between the data sets obtained at different temperatures (Figure 5D). In contrast to what we observed in the homozygous deletion screen, both the 30°C and 37°C heterozygous data sets were similarly enriched in ORFs involved in cellular transport (i.e., vesicle-mediated transport, Golgi apparatus, endoplasmic reticulum, vacuole; Figure 5D). These may reflect the enhanced dependence of essential genes on Hsp90 or may result from the different nature of this screen, which examines sensitivity to Hsp90 under conditions where at least half of the gene dosage is available. Importantly, screening the heterozygous deletion collection confirmed our previous findings that Hsp90 inhibition has widespread effects on the secretory pathway.

Taking advantage of our extensive data set of essential and nonessential targets of Hsp90, we next constructed a comprehensive map of Hsp90-secretory pathway interactions (Figure 6A). Graph-theoretical analysis combined all curated physical and genetic interactions with the genes in our homozygous and heterozygous data sets corresponding to the GO biological process classifications for either “secretory pathway” or “vesicle-mediated transport,” or the GO subcellular compartment classification for “endoplasmic reticulum.” The resulting Hsp90-secretory pathway interaction network contains 113 ORFs and 417 interactions. This network analysis underscored our previous observation that Hsp90 functions in virtually every aspect of the exocytic and endocytic secretory pathway. Many defined complexes, processes, and types of enzymes were identified as Hsp90 targets (Tables S7 and S9). Prominent among the targets were multisubunit complexes, including ESCRT I, II, and III; AP-adaptor complexes; and components of the vesicle-tethering COG and TRAPP complexes (Table S7 and Figures 6A, 6B, and 6D). Another noteworthy class of targets were transport-related GTPases, including the Rab-like *VPS21*, *YPT6*, *YPT7*, *YPT32*, *ARL1*, *ARL3*, *ARF1*, and *SEC4*, consistent with previous studies indicating that Hsp90 is required for Rab1 and Rab3a recycling in mammalian cells (Sakisaka et al., 2002; Chen and Balch, 2006). Notably, while these previous studies identified GDI as an additional target of Hsp90, we only observed the essential *GDI1* gene in positions 2932/5467 and 1998/5576 in the heterozygous 30°C and 37°C ranked data, respectively (Table S8). It is likely that the heterozygous screen is insensitive to impairment of genes, such as GDI, that act catalytically, and thus may be less affected by gene dosage. Another interesting

class of Hsp90 targets comprised components of the UPR and ERAD pathways, including the kinase IRE1 and its effector HAC1, as well as *HRD1*, *CUE1*, and various ER Hsp40-type cochaperones such as *ERJ5*, *JEM1*, *SCJ1*, and *HLJ1*. These latter findings link ER folding and quality control, as well as the sensing of ER stress, to the cytosolic Hsp90 chaperone machinery.

The surprising diversity of Hsp90 targets within the secretory pathway raises the possibility that Hsp90 exerts its action on different aspects of this pathway through direct interaction with multiple proteins and complexes. Alternatively, Hsp90 could act by interacting with a single family of effectors, such as Rabs, with pleiotropic activities. To distinguish between these possibilities, we used curated protein interaction maps obtained by proteomic analysis of *S. cerevisiae* complexes to determine the range of physical interactions between the secretory pathway Hsp90 targets from our screen and the Hsp90 chaperone machinery (Figure 6B). This network analysis revealed that Hsp90 and its chaperone cofactors interact directly with a wide spectrum of Hsp90 targets with different structural and functional properties, including Cog6p, Vps28p, Hrd1p, Apl2p, and Erg1p, as well as several Rab proteins (Figure 6B). This analysis supports the idea that Hsp90 exerts its function through direct physical interaction with many different components of the secretory pathway. Notably, the subunits of several multiprotein complexes involved in vesicle tethering (COG and TRAPP complexes) or endosome/vacuole transport (ESCRT I, II, and III complexes) were present in the Hsp90 physical interaction network (highlighted in Figure 6B). Because many of these complexes are highly dynamic and undergo highly regulated assembly/disassembly cycles during vesicle trafficking, it is tempting to speculate that Hsp90 may mediate their assembly or modulate their conformational cycle.

The Hsp90 physical interaction network was surprisingly sparse, suggesting that existing global proteomic analyses only detect a small subset of cellular physical interactions. We next used the COG complex to test this possibility. The COG complex is composed of two subcomplexes, lobe A and lobe B (Figure 6C; Ungar et al., 2002). Intriguingly, all the COG subunits in lobe B were found in our screen (Table S7). In contrast, only Cog6p contacted Hsp90 in the physical interaction network based on published proteomic studies (Figure 6B). We thus examined whether Hsp90 also interacts with the remaining three lobe B COG subunits (Figure 6C). Affinity isolation of GST-tagged COG subunits followed by immunoblot analysis for Hsp90 demonstrated that Hsp90 physically interacts with COG complex lobe B subunits Cog5p, Cog7p, and Cog8p (Figure 6B). The observation that all lobe B subunits revealed in our screen interact with Hsp90 suggests that this chaperone may participate in intralobe B or interlobe COG complex assembly. Furthermore, our analysis indicates that a more thorough physical interaction analysis, geared to stabilize labile Hsp90 interactions, will be required to elucidate the full range of cellular Hsp90 substrates.

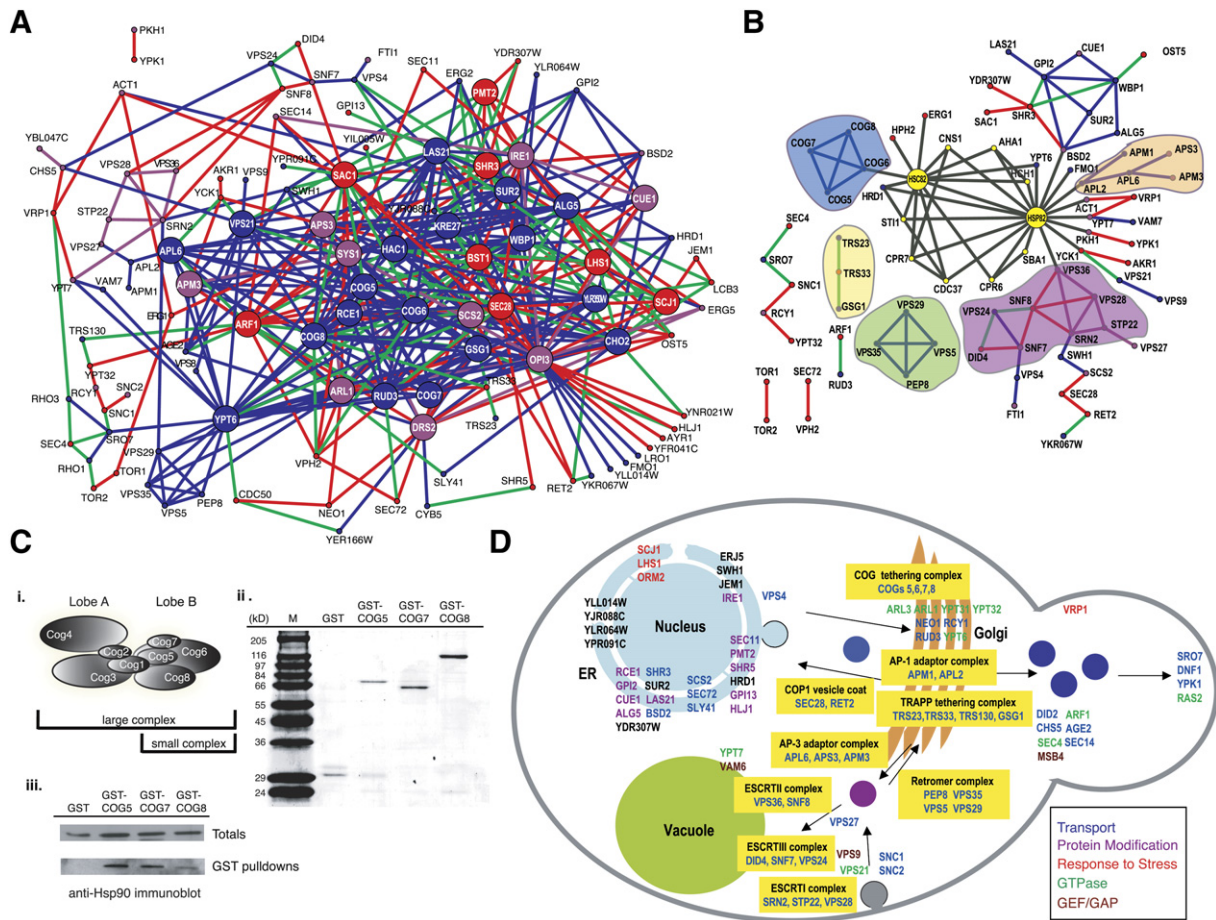


Figure 6. Whole-Genome Analysis of Secretory Pathway Genes Affected by Hsp90 Inhibition

(A) Hsp90-secretory pathway interaction network generated from curated protein-protein and genetic interactions related to the secretory pathway (see Results for details) within the homozygous and heterozygous 30°C and 37°C data sets. For labeling details, refer to Figure 3A legend. (B) Physical Hsp90-secretory pathway network. Only curated physical interactions are included. Hsp90 (HSC82 and HSP82 in enlarged yellow nodes) and well-established Hsp90 cochaperones are connected by gray edges. For other labeling details, refer to the legend for Figure 3A. Transport-related complexes are highlighted with overlays: blue, COG complex; yellow, TRAPP complex; green, retromer complex; purple, ESCRT I, II, and III complexes; orange, AP-1 and AP-3 adaptor complexes. (C) Scheme of the bilobular COG complex. (Ci) and (Cii) Glutathione-affinity isolation of complexes from yeast expressing GST or GST-COG5, -7, or -8 fusion proteins, separated by SDS-PAGE and stained with Coomassie blue (Cii). (Ciii) Total extracts (10 µg each lane) or affinity-isolated proteins were transferred to nitrocellulose, and Hsp90 was detected with anti-Hsp90 polyclonal antisera. (D) Schematic representation of points of action of Hsp90 in the secretory pathway from our analysis.

DISCUSSION

Multiple Cellular Functions of Hsp90

Our analysis revealed differences in the cellular processes sensitive to Hsp90 impairment at normal and elevated growth temperatures, indicating that the essential functions of Hsp90 change according to the needs of the cell. For example, while vesicle-mediated transport was significantly enriched in both 30°C and 37°C data sets, Hsp90 inhibition affected this process more profoundly under normal growth conditions (Figure 2C). At elevated temperatures, however, Hsp90 inhibition proved more detrimental for ORFs important for the G1 phase of the

cell cycle, signal transduction, and cytokinesis (Table S3 and Figure 2C). Interestingly, Hsp90 has previously been linked to kinetochore assembly in yeast (Bansal et al., 2004; Lingelbach and Kaplan, 2004; Stemmann et al., 2002). Most components involved in kinetochore assembly are essential for viability and thus not present in the homozygous deletion collection. However, our heterozygous deletion collection screen revealed several essential kinetochore components as extremely sensitive to Hsp90 inhibition (SKP1 and CTF13 rank in the top 5% at both 30°C and 37°C; SGT1 is in the top 5% at 30°C). Consistent with these findings, SGT1 has been reported to physically link Hsp90 to SKP1 (Catlett and Kaplan, 2006). Further,

instance, many aspects of vesicular transport and protein trafficking involve the ordered assembly and disassembly of large multisubunit complexes (Figure 7). The enrichment in complex-forming proteins in our 30°C data set prompts us to speculate that Hsp90 stabilizes subunits of these complexes prior to assembly or facilitates their conformational transitions during either binding or removal of these large hydrophobic complexes from membranes. Similarly, many components of the microtubule organizing center and kinetochores undergo ordered assembly and disassembly processes. During stress, e.g., at elevated temperatures, Hsp90 likely stabilizes labile conformations of many proteins, most notably cell cycle components (Figure 7).

In addition to Hsp90, other chaperone systems function in the eukaryotic cytosol (Frydman, 2001; Young et al., 2004). For example, the TRiC/CCT and GimC/Prefoldin chaperones interact with newly synthesized proteins and assist their folding to the native state. While Hsp90 is believed to act downstream of initial folding attempts, our data sets reveal an interaction of Hsp90 with two subunits of GimC, *GIM4* and *PFD1*. Genetic interactions between Hsp90 and another subunit, *GIM3*, have been reported (Tong et al., 2004). Further, many sensitive deletion strains uncovered in our screen exhibit interactions with *GIM4* in our network analysis (Figure 3AB). These results suggest a link between the GimC/Prefoldin chaperone and Hsp90. Further studies should clarify the interplay between these chaperone systems. For instance, they could carry out partially redundant functions. Alternatively, loss of GimC could impair folding of some newly made proteins, rendering them hyperdependent on the posttranslational assistance of Hsp90. We also find several links between Hsp90 and ER folding and quality control components. In principle this could reflect the cooperation between the cytosolic chaperone machinery and ER chaperones in the folding and maturation of transmembrane proteins with both cytosolic and luminal domains, as shown recently for CFTR (Wang et al., 2006), as well as the role of cytosolic chaperones in the degradation of retrotranslocated ERAD substrates (Meusser et al., 2005).

In sum, our combined systems approach identified novel Hsp90-dependent processes and may open the way to uncover novel functions for the numerous other components of the folding and quality control machineries.

EXPERIMENTAL PROCEDURES

Growth of Yeast Deletion Collections

Homozygous diploid deletion strains in the BY4743 background (Brachmann et al., 1998) were used in all experiments. The systematic construction of the deletion strains and the deletion pools have been previously described (Giaever et al., 1999, 2002). Pooled homozygous deletion strains were grown for ten generations in the absence (DMSO; no drug control) or presence of MII (200 μ M and 400 μ M; mabcetin II courtesy of the National Cancer Institute), and equivalent numbers of cells were sampled and frozen at -80° C. Genomic DNA was prepared from these samples, and the deletion strain-specific molecular barcodes were amplified by PCR. For details of growth, genomic DNA isola-

tion, primer sequences, and PCR conditions, see the Supplemental Data.

Array Hybridization and Preliminary Analysis

Amplified UPTAG and DOWNTAG sequences were combined and used to probe high-density oligonucleotide arrays containing probes complementary to the yeast deletion tags (Tag3 arrays, Affymetrix, Santa Clara) as previously described (Giaever et al., 1999, 2002). For details, see the Supplemental Data. Processed arrays were visualized with an Affymetrix scanner, and the intensity of each element on the array was calculated (CEL file). Affymetrix CEL files were then imported into a custom Matlab (Mathworks) software package for analysis and the *Rv* computed as described in the Supplemental Data. The ranked deletion strains were then plotted versus their average *Rv*. The early linear phase of the graph represents the strains most negatively affected by Hsp90 inhibition, and a cutoff was drawn accordingly constituting the top 5% of sensitive deletion strains.

Broad Characterization of Hsp90 Targets Using GO and GO Slim Assignments

The GO database (Harris et al., 2004) was utilized to collect a list of GO categories. In these classifications, gene products can be affiliated with one or more GO category assignments. These assignments were first used to look for enriched cellular components, functions, and processes in our experimental Hsp90 target data sets (see Table S4). We then determined the molecular function, biological process, and cellular component for each yeast protein according to its GO Slim annotations (Harris et al., 2004; Dwight et al., 2004). For details, see the Supplemental Data.

Yeast Interaction Network and Hsp90 Target Subnetwork

Yeast physical and genetic interactions are taken from the BioGRID database (Stark et al., 2006). From these interactions, we established a list of known Hsp90 interactors, defined as the core Hsp90 interactome of cofactors (*HSP82*, *HSC82*, *CNS1*, *CPR6*, *CPR7*, *STI1*, *SBA1*, *AHA1*, *HCH1*, *CDC37*), as well as the interaction partners for each of these genes. The resulting “known” Hsp90 interactors comprise 750 genes, 468 of which are known to be nonessential. Among these nonessential genes, 415 were tested at 30°C, and 458 were tested at 37°C.

Visualization and Analysis of the Hsp90 Target Subnetwork

The experimental network was visualized using Pajek (Batagelj and Mrvar, 1998). Several statistical and graph-theoretic analyses were performed for Hsp90 targets in relation to the yeast interaction network as described in the Supplemental Data.

Determining Enriched Features in Hsp90 Targets

Pfam, a database for protein domain and family classification (Bateman et al., 2004), was used to determine what types of proteins most commonly occurred in our data sets. Complex formers were defined using the MIPS (Mewes et al., 2004) complex catalog. For this analysis, an interaction between two proteins was assumed if the proteins belonged to the same complex. A complex former was then defined as a protein having more than one established interaction partner. The statistical analysis used to determine whether a particular protein feature is enriched in Hsp90 targets is described in detail in the Supplemental Data.

GST Pulldown Experiments

Yeast expressing GST alone or GST-COG5, -7, or -8 fusion proteins (courtesy of Michael Snyder; the GST-COG6 construct from this resource does not express a protein of the correct size and was therefore excluded from this analysis) were lysed in GST buffer (25 mM Tris [pH 8.0], 150 mM NaCl, 5 mM MgCl₂, 1 mM EDTA, 2.5% glycerol, 1 mM DTT, 0.1% Triton X-100, and protease inhibitors), and pulldowns containing 25 μ l of GST-Sepharose (Amersham Pharmacia Biotech,

Piscataway, NJ) slurry and 2 mg of protein in a total volume of 350 μ l were rotated at 4°C for 20 min. Isolated proteins were resolved on 12% SDS-PAGE gels and either Coomassie blue stained or transferred to nitrocellulose and probed with anti-Hsp90 antisera (kind gift of Avrom Caplan).

Fluorescence Microscopy

Yeast transformed with a GPS-GFP construct (courtesy of Scott Emr) were grown overnight at 30°C to mid-log phase ($OD_{600} = 0.5\text{--}0.8$). Conventional GFP fluorescence micrographs were obtained using a Zeiss Axiovert 200M microscope. For details, see the [Supplemental Data](#).

Invertase Activity Assay

This experiment was performed essentially as previously described (Luk and Culotta, 2001; Poon et al., 1999). For details, see the [Supplemental Data](#).

Cell Cycle Synchronization and Flow Cytometry

Yeast were synchronized in 150 mM hydroxyurea for 3.5 hr., released for 2 hr, and subjected to FACS analysis on an FHCRC Becton Dickinson machine. Samples of the same cells were analyzed by microscopy to observe propidium iodide-labeled DNA. For experimental details see the [Supplemental Data](#).

Supplemental Data

The Supplemental Data include Supplemental Experimental Procedures, three figures, and nine tables and can be found with this article online at <http://www.cell.com/cgi/content/full/131/1/121/DC1>.

ACKNOWLEDGMENTS

We thank Drs. Susan Lindquist, Avrom Caplan, Scott Emr, and Michael Snyder for their generous contributions of antibodies, strains, and/or plasmids. We also thank Allyson O'Donnell for advice and reagents for the invertase activity assay. This work was supported by NIH grant GM56433. A.J.M. was a recipient of postdoctoral fellowship NRSA GM64992 from the NIH. Y.X. was supported by a postdoctoral fellowship from the Jane Coffin Childs Memorial Fund for Medical Research. M.G. is supported by a grant from NIH/NIGMS (5P50GM062413-03). J.F. and M.G. were Distinguished Young Keck Scholars.

Received: June 13, 2006

Revised: May 18, 2007

Accepted: July 20, 2007

Published: October 4, 2007

REFERENCES

Bansal, P.K., Abdulle, R., and Kitagawa, K. (2004). Sgt1 associates with Hsp90: An initial step of assembly of the core kinetochore complex. *Mol. Cell. Biol.* *24*, 8069–8079.

Batagelj, V., and Mrvar, A. (1998). Pajek—Program for large network analysis. *Connections* *21*, 47–57.

Bateman, A., Coin, L., Durbin, R., Finn, R.D., Hollich, V., Griffiths-Jones, S., Khanna, A., Marshall, M., Moxon, S., Sonnhammer, E.L., et al. (2004). The Pfam protein families database. *Nucleic Acids Res.* *32*, D138–D141.

Bohen, S.P. (1998). Genetic and biochemical analysis of p23 and ansamycin antibiotics in the function of Hsp90-dependent signaling proteins. *Mol. Cell. Biol.* *18*, 3330–3339.

Brachmann, C.B., Davies, A., Cost, G.J., Caputo, E., Li, J., Hieter, P., and Boeke, J.D. (1998). Designer deletion strains derived from *Saccharomyces cerevisiae* S288C: A useful set of strains and plasmids for PCR-mediated gene disruption and other applications. *Yeast* *14*, 115–132.

Buchner, J. (1999). Hsp90 & Co.—A holding for folding. *Trends Biochem. Sci.* *24*, 136–141.

Catlett, M.G., and Kaplan, K.B. (2006). Sgt1p is a unique co-chaperone that acts as a client adaptor to link Hsp90 to Skp1p. *J. Biol. Chem.* *281*, 33739–33748.

Chen, C.Y., and Balch, W.E. (2006). The Hsp90 chaperone complex regulates GDI-dependent Rab recycling. *Mol. Biol. Cell* *17*, 3494–3507.

Chiosis, G., and Neckers, L. (2006). Tumor selectivity of Hsp90 inhibitors: The explanation remains elusive. *ACS Chem. Biol.* *1*, 279–284.

de Carcer, G. (2004). Heat shock protein 90 regulates the metaphase-anaphase transition in a polo-like kinase-dependent manner. *Cancer Res.* *64*, 5106–5112.

Deutschbauer, A.M., Jaramillo, D.F., Proctor, M., Kumm, J., Hillenmeyer, M.E., Davis, R.W., Nislow, C., and Giaever, G. (2005). Mechanisms of haploinsufficiency revealed by genome-wide profiling in yeast. *Genetics* *169*, 1915–1925.

Dwight, S.S., Balakrishnan, R., Christie, K.R., Costanzo, M.C., Dolinski, K., Engel, S.R., Feierbach, B., Fisk, D.G., Hirschman, J., Hong, E.L., et al. (2004). *Saccharomyces cerevisiae* genome database: Underlying principles and organization. *Brief. Bioinform.* *5*, 9–22.

Fortugno, P., Beltrami, E., Plescia, J., Fontana, J., Pradhan, D., Marchisio, P.C., Sessa, W.C., and Altieri, D.C. (2003). Regulation of survivin function by Hsp90. *Proc. Natl. Acad. Sci. USA* *100*, 13791–13796.

Frydman, J. (2001). Folding of newly translated proteins in vivo: The role of molecular chaperones. *Annu. Rev. Biochem.* *70*, 603–647.

Giaever, G. (2003). A chemical genomics approach to understanding drug action. *Trends Pharmacol. Sci.* *24*, 444–446.

Giaever, G., Shoemaker, D.D., Jones, T.W., Liang, H., Winzler, E.A., Astromoff, A., and Davis, R.W. (1999). Genomic profiling of drug sensitivities via induced haploinsufficiency. *Nat. Genet.* *21*, 278–283.

Giaever, G., Chu, A.M., Ni, L., Connelly, C., Riles, L., Veronneau, S., Dow, S., Lucau-Danila, A., Anderson, K., Andre, B., et al. (2002). Functional profiling of the *Saccharomyces cerevisiae* genome. *Nature* *418*, 387–391.

Harris, M.A., Clark, J., Ireland, A., Lomax, J., Ashburner, M., Foulger, R., Eilbeck, K., Lewis, S., Marshall, B., Mungall, C., et al. (2004). The Gene Ontology (GO) database and informatics resource. *Nucleic Acids Res.* *32*, D258–D261.

Hettema, E.H., Valdez-Taubas, J., and Pelham, H.R. (2004). Bsd2 binds the ubiquitin ligase Rsp5 and mediates the ubiquitination of transmembrane proteins. *EMBO J.* *23*, 1279–1288.

Katzmann, D.J., Stefan, C.J., Babst, M., and Emr, S.D. (2003). Vps27 recruits ESCRT machinery to endosomes during MVB sorting. *J. Cell Biol.* *162*, 413–423.

Lange, B.M., Rebollo, E., Herold, A., and Gonzalez, C. (2002). Cdc37 is essential for chromosome segregation and cytokinesis in higher eukaryotes. *EMBO J.* *21*, 5364–5374.

Lingelbach, L.B., and Kaplan, K.B. (2004). The interaction between Sgt1p and Skp1p is regulated by HSP90 chaperones and is required for proper CBF3 assembly. *Mol. Cell. Biol.* *24*, 8938–8950.

Liu, X.F., and Culotta, V.C. (1994). The requirement for yeast superoxide dismutase is bypassed through mutations in BSD2, a novel metal homeostasis gene. *Mol. Cell. Biol.* *14*, 7037–7045.

Luk, E.E., and Culotta, V.C. (2001). Manganese superoxide dismutase in *Saccharomyces cerevisiae* acquires its metal co-factor through a pathway involving the Nrapm metal transporter, Smf2p. *J. Biol. Chem.* *276*, 47556–47562.

Meusser, B., Hirsch, C., Jarosch, E., and Sommer, T. (2005). ERAD: The long road to destruction. *Nat. Cell Biol.* *7*, 766–772.

Mewes, H.W., Amid, C., Arnold, R., Frishman, D., Guldener, U., Mannhaupt, G., Munsterkotter, M., Pagel, P., Strack, N., Stumpfen,

- V., et al. (2004). MIPS: Analysis and annotation of proteins from whole genomes. *Nucleic Acids Res.* 32, D41–D44.
- Millson, S.H., Truman, A.W., King, V., Prodromou, C., Pearl, L.H., and Piper, P.W. (2005). A two-hybrid screen of the yeast proteome for Hsp90 interactors uncovers a novel Hsp90 chaperone requirement in the activity of a stress-activated mitogen-activated protein kinase, Slt2p (Mpk1p). *Eukaryot. Cell* 4, 849–860.
- Mimnaugh, E.G., Xu, W., Vos, M., Yuan, X., and Neckers, L. (2006). Endoplasmic reticulum vacuolization and valosin-containing protein relocalization result from simultaneous hsp90 inhibition by geldanamycin and proteasome inhibition by velcade. *Mol. Cancer Res.* 4, 667–681.
- Nathan, D.F., Vos, M.H., and Lindquist, S. (1997). In vivo functions of the *Saccharomyces cerevisiae* Hsp90 chaperone. *Proc. Natl. Acad. Sci. USA* 94, 12949–12956.
- Nomura, M., Nomura, N., Newcomb, E.W., Lukyanov, Y., Tamasdan, C., and Zagzag, D. (2004). Geldanamycin induces mitotic catastrophe and subsequent apoptosis in human glioma cells. *J. Cell. Physiol.* 201, 374–384.
- Odorizzi, G., Katzmann, D.J., Babst, M., Audhya, A., and Emr, S.D. (2003). Bro1 is an endosome-associated protein that functions in the MVB pathway in *Saccharomyces cerevisiae*. *J. Cell Sci.* 116, 1893–1903.
- Pearl, L.H., and Prodromou, C. (2006). Structure and mechanism of the Hsp90 molecular chaperone machinery. *Annu. Rev. Biochem.* 75, 271–294.
- Picard, D. (2002). Heat-shock protein 90, a chaperone for folding and regulation. *Cell. Mol. Life Sci.* 59, 1640–1648.
- Picard, D. (2006). Chaperoning steroid hormone action. *Trends Endocrinol. Metab.* 17, 229–235.
- Picard, D., Khurshed, B., Garabedian, M.J., Fortin, M.G., Lindquist, S., and Yamamoto, K.R. (1990). Reduced levels of hsp90 compromise steroid receptor action in vivo. *Nature* 348, 166–168.
- Piper, R.C., Cooper, A.A., Yang, H., and Stevens, T.H. (1995). VPS27 controls vacuolar and endocytic traffic through a prevacuolar compartment in *Saccharomyces cerevisiae*. *J. Cell Biol.* 131, 603–617.
- Poon, P.P., Cassel, D., Spang, A., Rotman, M., Pick, E., Singer, R.A., and Johnston, G.C. (1999). Retrograde transport from the yeast Golgi is mediated by two ARF GAP proteins with overlapping function. *EMBO J.* 18, 555–564.
- Pratt, W.B., and Toft, D.O. (2003). Regulation of signaling protein function and trafficking by the hsp90/hsp70-based chaperone machinery. *Exp. Biol. Med.* 228, 111–133.
- Ryan, P.E., Davies, G.C., Nau, M.M., and Lipkowitz, S. (2006). Regulating the regulator: Negative regulation of Cbl ubiquitin ligases. *Trends Biochem. Sci.* 31, 79–88.
- Sakisaka, T., Meerlo, T., Matteson, J., Plutner, H., and Balch, W.E. (2002). Rab- α GDI activity is regulated by a Hsp90 chaperone complex. *EMBO J.* 21, 6125–6135.
- Sangster, T.A., Lindquist, S., and Queitsch, C. (2004). Under cover: Causes, effects and implications of Hsp90-mediated genetic capacitance. *Bioessays* 26, 348–362.
- Stark, C., Breitkreutz, B.J., Reguly, T., Boucher, L., Breitkreutz, A., and Tyers, M. (2006). BioGRID: A general repository for interaction datasets. *Nucleic Acids Res.* 34, D535–D539.
- Stemann, O., Neidig, A., Kocher, T., Wilm, M., and Lechner, J. (2002). Hsp90 enables Ctf13p/Skp1p to nucleate the budding yeast kinetochore. *Proc. Natl. Acad. Sci. USA* 99, 8585–8590.
- Thompson, B.J., Mathieu, J., Sung, H.H., Loeser, E., Rorth, P., and Cohen, S.M. (2005). Tumor suppressor properties of the ESCRT-II complex component Vps25 in *Drosophila*. *Dev. Cell* 9, 711–720.
- Tong, A.H., Lesage, G., Bader, G.D., Ding, H., Xu, H., Xin, X., Young, J., Berriz, G.F., Brost, R.L., Chang, M., et al. (2004). Global mapping of the yeast genetic interaction network. *Science* 303, 808–813.
- Ungar, D., Oka, T., Brittle, E.E., Vasile, E., Lupashin, V.V., Chatterton, J.E., Heuser, J.E., Krieger, M., and Waters, M.G. (2002). Characterization of a mammalian Golgi-localized protein complex, COG, that is required for normal Golgi morphology and function. *J. Cell Biol.* 157, 405–415.
- Vaughan, C.K., Gohlke, U., Sobott, F., Good, V.M., Ali, M.M., Prodromou, C., Robinson, C.V., Saibil, H.R., and Pearl, L.H. (2006). Structure of an Hsp90-Cdc37-Cdk4 complex. *Mol. Cell* 23, 697–707.
- Wang, X., Venable, J., LaPointe, P., Hutt, D.M., Koulov, A.V., Copping, J., Gurkan, C., Kellner, W., Matteson, J., Plutner, H., et al. (2006). Hsp90 cochaperone Aha1 downregulation rescues misfolding of CFTR in cystic fibrosis. *Cell* 127, 803–815.
- Wegele, H., Müller, L., and Buchner, J. (2004). Hsp70 and Hsp90—A relay team for protein folding. *Rev. Physiol. Biochem. Pharmacol.* 151, 1–44.
- Whitesell, L., and Lindquist, S.L. (2005). HSP90 and the chaperoning of cancer. *Nat. Rev. Cancer* 5, 761–772.
- Winzeler, E.A., Shoemaker, D.D., Astromoff, A., Liang, H., Anderson, K., Andre, B., Bangham, R., Benito, R., Boeke, J.D., Bussey, H., et al. (1999). Functional characterization of the *S. cerevisiae* genome by gene deletion and parallel analysis. *Science* 285, 901–906.
- Young, J.C., Moarefi, I., and Hartl, F.U. (2001). Hsp90: A specialized but essential protein-folding tool. *J. Cell Biol.* 154, 267–273.
- Young, J.C., Agashe, V.R., Siegers, K., and Hartl, F.U. (2004). Pathways of chaperone-mediated protein folding in the cytosol. *Nat. Rev. Mol. Cell Biol.* 5, 781–791.
- Zhao, R., Davey, M., Hsu, Y.C., Kaplanek, P., Tong, A., Parsons, A.B., Krogan, N., Cagney, G., Mai, D., Greenblatt, J., et al. (2005). Navigating the chaperone network: An integrative map of physical and genetic interactions mediated by the hsp90 chaperone. *Cell* 120, 715–727.